Ge-on-Si single photon avalanche diode performance enhancement with photonic crystal nano-hole arrays

Charlie McCarthy†, Charlie Smith†, Hannah Mowbray, Douglas J. Paul, and Ross W. Millar

James Watt School of Engineering, University of Glasgow, Glasgow G12 8LT, Scotland, United Kingdom
† These authors contributed equally to the work.

ABSTRACT

Germanium-on-silicon (Ge-on-Si) single photon avalanche diodes (SPADs) operating in the short-wave infrared (SWIR) have various applications such as long-range eye-safe LIDAR, quantum imaging, and quantum key distribution. These SPADs offer compatibility with Si foundries and potential cost advantages over existing InGaAs/InP devices. However, cooling is necessary to reduce dark-count rates (DCR), which limits photon absorption at 1550 nm wavelength. To address this, we propose integrating a photonic crystal (PC) nano-hole array structure on the Ge absorber layer. While this technique has shown enhanced responsivity in linear Ge detectors, its potential in Ge-on-Si SPADs remains unexplored. Our simulations consider temperature dependence and the impact of electric-field hot-spots on dark count rates. Through these simulations, we have identified means of enhancing single-photon detection efficiency (SPDE) without adversely affecting DCR. We predict significant improvements in performance, including at least a 2.5x enhancement in absorption efficiency.

Keywords: Ge-on-Si, SPAD, Photonic Crystal, Absorption Enhancement, Simulation

1. INTRODUCTION

Single Photon Avalanche Diodes (SPADs) are devices designed to precisely measure the arrival of individual incident photons, typically with sub-ns timing resolution.[1] They find extensive use in various applications, including long range eye-safe LIDAR,[2] quantum-key distribution[3] (QKD) and fluorescence lifetime imaging.[4] For LIDAR applications, for example, operation within the short-wave infrared (SWIR) wavelengths are preferred for three main reasons: reduced solar background radiation, resulting in lower ambient light noise and a higher signal-to-noise ratio (SNR);[5] the ability to use higher laser powers, up to ∼20 times compared to near-infrared (NIR), while maintaining eye safety;[6] and improved imaging through atmospheric obscurrants such as smoke and fog.[7–9] SWIR operation is therefore crucial for extending detection range in LIDAR systems and also for integrating with telecommunication networks in quantum applications such as QKD.

The exploration of Group IV materials for SPADs operating in the SWIR has been a subject of investigation for several years, and we have previously demonstrated novel pseudo-planar germanium-on-silicon SPADs with absorption into the SWIR,[10–12] which offer these capabilities at potentially significantly lower costs compared to InGaAs/InP SPADs, which is the state-of-the-art SPAD technology in this wavelength range. This cost reduction is attributed to compatability with silicon foundries and the ease of integration with CMOS electronics.

We have demonstrated Single Photon Detection Efficiencies (SPDEs) of up to 38% at a wavelength of 1310 nm. Subsequently, a scaled 26 μm diameter device[11] demonstrated a record-low noise-equivalent power of 7.7×10^{-17} $W/Hz^{0.5}$, and these devices successfully facilitated LIDAR measurements in laboratory conditions[13,14] up to 1450 nm wavelength. Currently, these devices are operated at wavelengths $\leq$ 1450 nm due to cooling constraints ($\leq$ 175 K) needed to minimise DCR. At these temperature a blue-shift in absorption causes a reduction in absorption at 1550 nm, which is the target wavelength of operation. Further to this, it would be desirable to operate the devices at 225 K or higher so they can be integrated with Peltier coolers for commercial applications that require compact, low power solutions. Optimizing the technology to reduce DCR will enable this higher temperature operation and hence increased absorption at 1550 nm, however even at 225 K, less than 10 % of photons are absorbed in a 1 μm thick Ge absorber layer.

For further author information send correspondence to R.W Millar (E-mail: ross.millar@glasgow.ac.uk)

Increasing SPDE can be achieved through the use of a thicker Ge absorber (≥ 2 μm), but this may results in an increased DCR due to the increased volume of the narrow bandgap germanium region. The proposed solution to enhance absorption is to integrate the SPAD structure with an etched Photonic Crystal (PC) structure, providing a method to overcome the challenges associated with improving SPDE without compromising DCR, hence balancing the performance requirements.

In recent years, etched nano-hole PC arrays have been utilized to enhance Ge-on-Si photodiode and APD structures' absorption[15–17] . These arrays provide resonant enhancement to laterally coupled and weakly guided modes within the Ge absorber layer. Importantly, they allow for a thinner absorption layer, ensuring rapid photo-carrier collection and maintaining high electrical bandwidths. However, lower internal electric fields and room temperature operating conditions mean less care needs to be shown for the design of such devices. Geiger mode devices like SPADs are sensitive to single carriers, and so differences in the leakage current and generation rate from the inclusion of a PC has the potential for a net negative performance. This is especially important with the enhanced trap assisted tunnelling (TAT) seen at lower device operating temperatures. The use of both optical and electrical simulation is therefore required to gain an understanding of the potential trade-offs between increasing single-photon detection efficiencies and increasing dark-count rates at anticipated operation temperatures. In the following work, a simulated SPAD layer stack consisting of p++ germanium contact layer, an intrinsic germanium absober and then an intrinsic silicon avalanche layer on an n++ silicon substrate is used. Between the two intrinsic layers is a locally implanted charge sheet, with a dose selected to optimise the electric field in both avalanche and multiplication regions.

2. OPTICAL SIMULATION

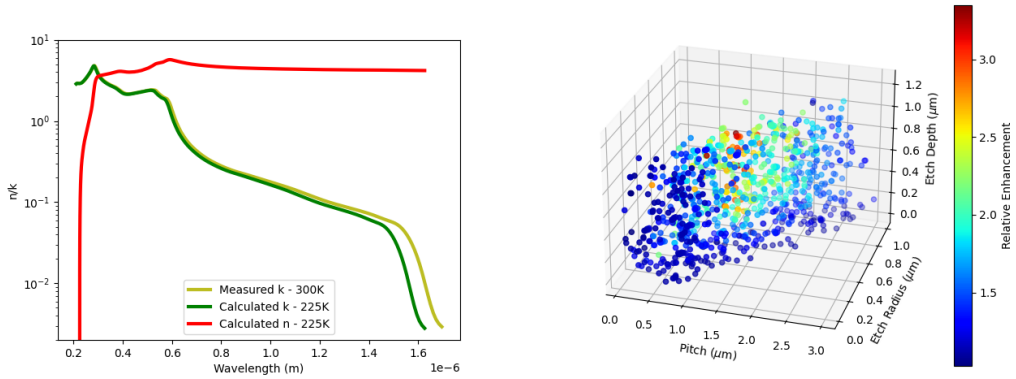

(a) (b)

Figure 1. (a) Calculated n & k data for 225 K using Varshni model and Kramers-Kronig transformation (b) An example of the 3D parameter space searched using the optimisation algorithm

The optical simulation was undertaken using the Lumerical Finite Difference Time Domain (FDTD) 3D Electromagnetic Simulator. We aimed to assess the increase in absorption power within the intrinsic germanium absorption layer resulting from the incorporation of a photonic crystal on the SPAD structure. The power absorbed was determined by analyzing the divergence of the Poynting vector. The Varshni model[18] was employed to account for the blue shift in absorption data measured by ellipsometry, due to the operation at 225 K, and the corresponding shift in refractive index was factored in through the application of the Kramers-Kronig transformation.[19] Initially, a simulation without an integrated photonic crystal was performed to calculate the absorbed power in germanium from a broadband Gaussian source (wavelength of 1.2 μm to 1.6 μm) above the structure. Subsequent simulations were compared to establish the relative absorption enhancement.

Optimization was performed using the constrained optimization by linear approximation (COBYLA)[20] algorithm to identify the geometry with maximal optical performance. The parameter space searched by the algorithm contained 3 variables; radius r, pitch p and etch depth d of the crystal. To expedite the lengthy simulation process, an infinite crystal lattice was employed initially. Subsequently, promising solutions were

further scrutinized on a finite 10x10 lattice of holes to validate the enhancement at a size comparable to the optical window of a device. Figure 1(b) shows the relative enhancement within a 3D plot of the parameter space, highlighting optimal PC parameters.

3. ELECTRICAL SIMULATION

An electrical simulation was completed using Synopsys Sentaurus to solve the Poisson and carrier continuity equations to model the electric field profiles within a SPAD. This data was then used to solve McIntyre model[21] for avalanche probability along the electric field lines, incorporating the Van Overstraeten and De Man avalanche coefficients.[22] The joint avalanche probability distribution for the entire device was calculated, representing the probability that a carrier pair generation at any specific location would lead to a self-sustaining avalanche event.

Calculation of the non-photogenerated carrier generation rate made use of a Shockley-Read-Hall (SRH) model along with the Hurkx Trap Assisted Tunneling (TAT) electric field model.[23] Band-to-band tunnelling was calculated[24] but was found to be insignificant for the electric fields present in the device. The DCR was then calculated by summing the product of the joint avalanche probability and generation rate over the entire device bulk and external surfaces.[25] A pseudo-3D simulation technique was used to fully capture the effect of the inclusion of the photonic crystal. A 360 degree cylindrical symmetry normally exists on these SPAD devices, allowing for a 2D simulation, however with the inclusion of the photonic crystal this cylindrical symmetry is broken. To overcome this, one periodic photonic crystal section was simulated and then substituted into the cylindrical 2D simulation in the correct pattern to mimic a full 3D simulation.

4. ETCHED PHOTONIC CRYSTAL INTO GE ABSORBER

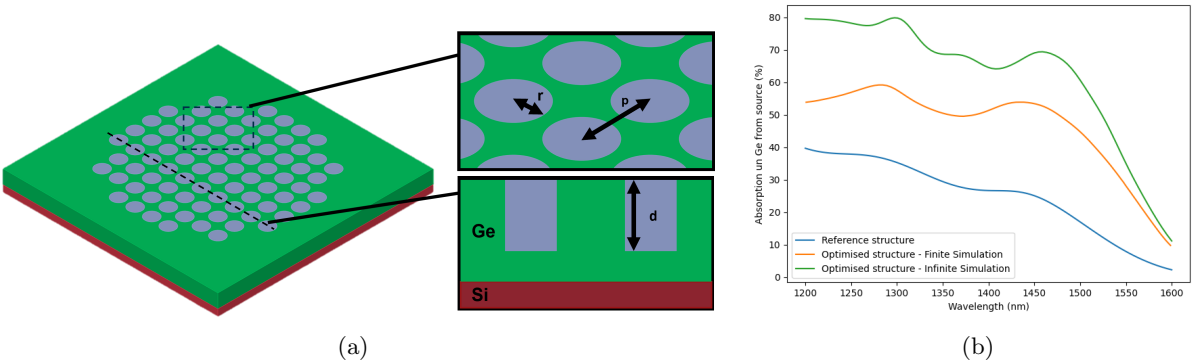

(a) (b)

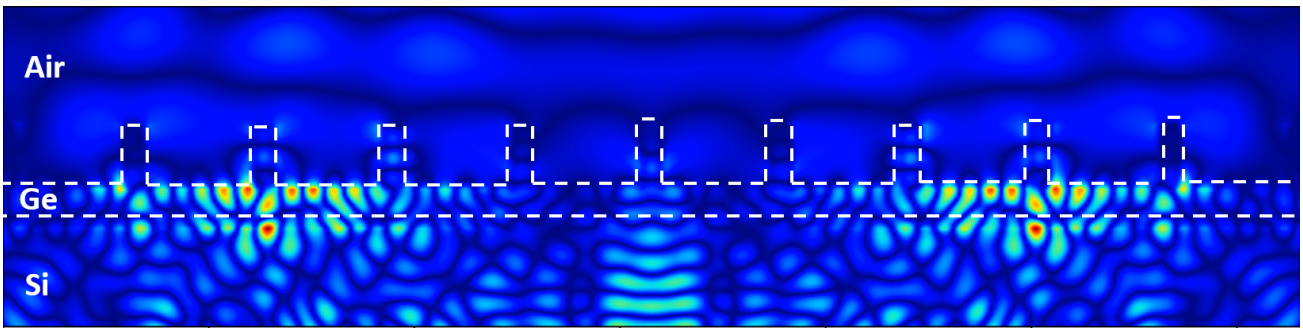

(c)

Figure 2. (a) Proposed structure for integrating photonic crystal with Ge absorber. (b) Absorption spectra for finite and infinite simulation, with reference device included to highlight improvement. (d) 2D cross-section of FDTD simulation showing lateral mode propagation.

The first enhancement method investigated was to integrate the photonic crystal directly into the germanium absorber by etching. The structure can be seen in Figure 2(a). The optimal parameters where determined as an etch radius of 514 nm, a pitch of 1262 nm, and an etch depth of 1000 nm. This configuration achieved a 3.4x absorption enhancement compared to an unetched reference structure at a wavelength of 1550 nm, resulting in 29% total absorption. Figure 2(b) and 2(c) illustrate the absorption spectra for the etched structure (finite and infinite simulations) compared to the reference structure, and the lateral mode propagation through the Ge absorber respectively. The coupling of power into these lateral modes effectively increases the layer's thickness, enhancing overall absorption in the layer stack.

Electrical simulation for the proposed enhancement method exhibits unfavorable outcomes, as the simulation predicts an increase in DCR for structures featuring etched holes directly within the germanium absorber. Figure 3(a) depicts a reverse bias-versus-relative DCR plot for the unetched reference structure and structures with varying etch depth. The blue line represents the normalized DCR for the reference structure, and all other plots are presented relative to this baseline starting at the breakdown bias of 46 V. It is evident that at increasing excess biases there is an increase in DCR for the etched devices, with deeper etches result in further diminished DCR performance. These etches in the active region of the device result in a non-uniform electric field and consequently lead to the formation of hot spots. This can be seen in the electric field profile of the device shown in Figure 3(b). Additionally, these etches contribute to an increased sidewall area, which is undesirable due to the higher density of trap states and defects. This elevated sidewall contribution means there is a greater chance of generating non-photogenerated carriers, adversely impacting the device performance.

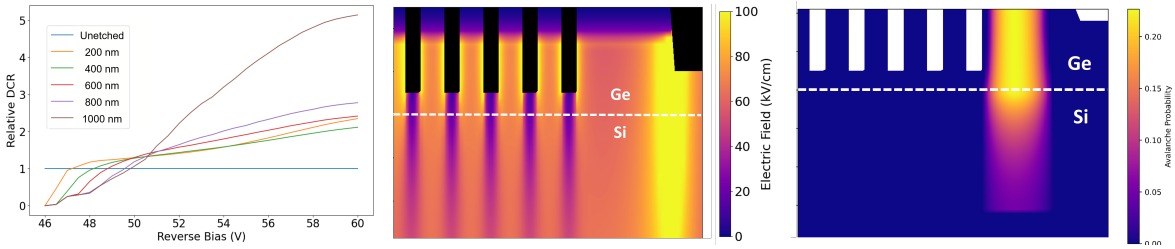

(a) (b) (c)

Figure 3. (a) Reverse bias-versus-relative DCR plot for the unetched reference structure and structures with varying etch depth. (b) Simulated electric field profile of an etched device (c) Avalanche probability map of an etched device, highlighting preferential edge breakdown.

Examination of the avalanche probability map (Fig. 3(c)) reveals preferential edge breakdown in the device, occurring prior to breakdown below the etched photonic crystal. This is due to nonuniform electric field in the device introduced by the etching of holes in the active area. The preferential edge breakdown implies that increased etch depths require higher excess bias levels for efficient photon detection. In scenarios where only the device's edge has broken down, triggering events solely involve non-photogenerated carriers. In other words, the avalanche probability becomes non-zero at the edge of the depletion region before the volume beneath the photonic crystal, containing the majority of absorbed power. Consequently, higher excess biases are needed for photodetection, resulting in prohibitively high DCR. This restricts device performance, lifespan, and necessitates the implementation of more complex readout electronics to address these limitations. While the combined SPDE and DCR are expected to result in an improvement to performance, the method demonstrates heightened vulnerability to fabrication variations and necessitates the use of elevated excess biases, mandating a more robust strategy.

5. ETCHED PHOTONIC CRYSTAL INTO AMORPHOUS SILICON LAYER

An alternative strategy was to incorporate a layer of amorphous silicon (α-Si) on top of the germanium absorber and etch the photonic crystal into this instead. α-Si is silicon foundry compatible, transparent at 1550 nm wavelengths and results in a high index contrast. An illustration of this structure can be seen in Figure 4(a). As detailed previously, we determined the optimal parameters of such a structure to be: an etch radius of 553 nm, a

pitch of 1249 nm, and an etch depth of 900 nm. Preliminary results from the infinite lattice for this configuration achieved a 3.0x absorption enhancement compared to an unetched reference structure at 1550nm wavelength, resulting in 26% total absorption. Figure 4(b) and 4(c) illustrate the absorption spectra for the etched structure compared to the reference structure, and the lateral mode propagation through the Ge absorber respectively.

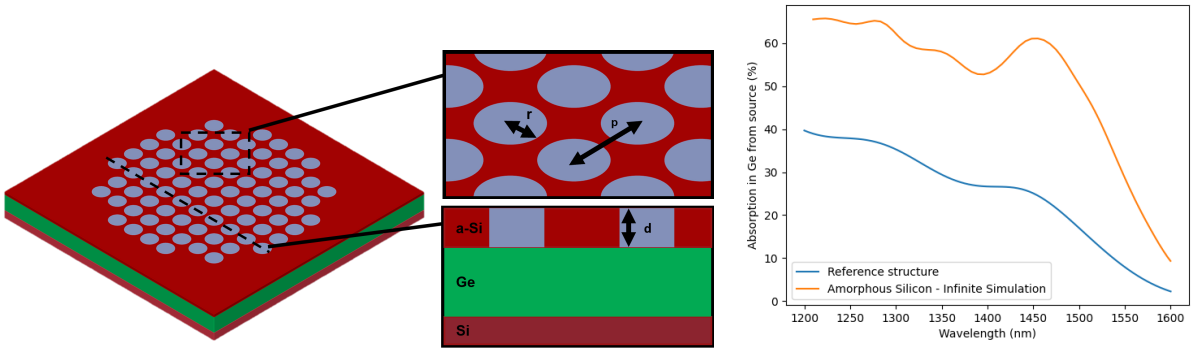

(a) (b)

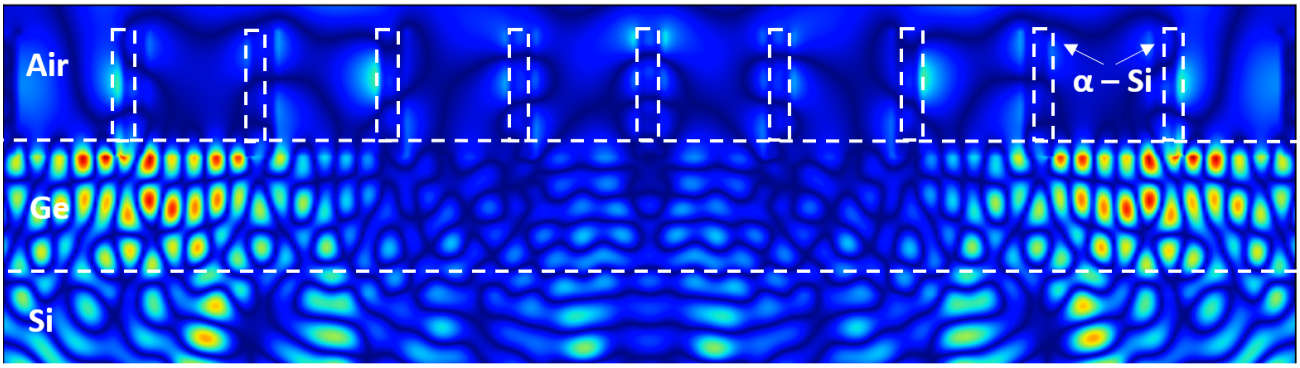

(c)

Figure 4. (a) Proposed structure for integrating α-Si photonic crystal with SPAD structure. (b) Absorption spectra for infinite simulation, with reference device included to highlight improvement. (c) 2D cross-section of FDTD simulation showing lateral mode propagation.

6. CONCLUSION AND FUTURE WORK

In this paper, the integration of a photonic crystal nano-hole array structure with a Ge-on-Si SPAD aimed at enhancing single-photon detection efficiency in the SWIR without compromising dark-count rates at elevated temperatures has been investigated using optical and electrical simulations. Direct integration of the photonic crystal into the germanium absorber increased absorption efficiency by 3.4x but led to an undesirable rise in DCR due to non-uniform electric fields and preferential edge breakdown. An alternative approach involved incorporating a layer of α-Si on top of the germanium absorber and etching the photonic crystal into this. Preliminary results on an infinite lattice showed a promising 3.0x absorption enhancement without significant DCR increase.

In the future, a spatial map of absorption will be calculated. This data will then be used alongside the spatial triggering probability distribution from electrical simulation to calculate SPDE. The calculation of Noise Equivalent Power will then be completed. NEP is an all-encompassing figure-of-merit that is a function of SPDE and DCR to comprehensively assess the net impact of the inclusion of the photonic crystal.

ACKNOWLEDGMENTS

Royal Academy of Engineering (RF-201819-18-187); Innovate UK (44835); Engineering and Physical Sciences Research Council (UK EPSRC; EP/S026428/1, EP/T001011/1, EP/T00097X/1).

REFERENCES

[1] Buller, G. S. and Collins, R. J., "Single-photon generation and detection," *Measurement Science and Technology* **21**, 012002 (nov 2009).

[2] McCarthy, A., Ren, X., Frera, A. D., Gemmell, N. R., Krichel, N. J., Scarcella, C., Ruggeri, A., Tosi, A., and Buller, G. S., "Kilometer-range depth imaging at 1550 nm wavelength using an ingaas/inp single-photon avalanche diode detector," *Opt. Express* **21**, 22098–22113 (Sep 2013).

[3] Zhang, J., Eraerds, P., Walenta, N., Barreiro, C., Thew, R., and Zbinden, H., "2.23 ghz gating ingaas/inp single-photon avalanche diode for quantum key distribution," in [*Advanced Photon Counting Techniques IV*], Itzler, M. A. and Campbell, J. C., eds., SPIE (Apr. 2010).

[4] Ulku, A. C., Bruschini, C., Antolovic, I. M., Kuo, Y., Ankri, R., Weiss, S., Michalet, X., and Charbon, E., "A 512 × 512 spad image sensor with integrated gating for widefield flim," *IEEE Journal of Selected Topics in Quantum Electronics* **25**, 1–12 (Jan. 2019).

[5] Eltbaakh, Y. A., Ruslan, M., Alghoul, M., Othman, M., Sopian, K., and Fadhel, M., "Measurement of total and spectral solar irradiance: Overview of existing research," *Renewable and Sustainable Energy Reviews* **15**, 1403–1426 (Apr. 2011).

[6] "Safety of laser products - part 1: Equipment classification and requirements," standard, International Electrotechnical Commission, Geneva, CH (Nov. 2007).

[7] Tobin, R., Halimi, A., McCarthy, A., Laurenzis, M., Christnacher, F., and Buller, G. S., "Three-dimensional single-photon imaging through obscurants," *Opt. Express* **27**, 4590–4611 (Feb 2019).

[8] Plosz, S., Maccarone, A., McLaughlin, S., Buller, G. S., and Halimi, A., "Real-time reconstruction of 3d videos from single-photon lidar data in the presence of obscurants," *IEEE Transactions on Computational Imaging* , 1–14 (2023).

[9] Tobin, R., Halimi, A., McCarthy, A., Soan, P. J., and Buller, G. S., "Robust real-time 3d imaging of moving scenes through atmospheric obscurant using single-photon lidar," *Scientific Reports* **11**, 11236 (2021).

[10] Vines, P., Kuzmenko, K., Kirdoda, J., Dumas, D. C., Mirza, M. M., Millar, R. W., Paul, D. J., and Buller, G. S., "High performance planar germanium-on-silicon single-photon avalanche diode detectors," *Nature Communications* **10** (2019).

[11] Llin, L. F., Kirdoda, J., Thorburn, F., Huddleston, L. L., Greener, Z. M., Kuzmenko, K., Vines, P., Dumas, D. C. S., Millar, R. W., Buller, G. S., and Paul, D. J., "High sensitivity Ge-on-Si single-photon avalanche diode detectors," *Opt. Lett.* **45**, 6406–6409 (Dec 2020).

[12] Thorburn, F. E., Huddleston, L. L., Kirdoda, J., Millar, R. W., Ferre-Llin, L., Yi, X., Paul, D. J., and Buller, G. S., "High efficiency planar geometry germanium-on-silicon single-photon avalanche diode detectors," in [*Advanced Photon Counting Techniques XIV*], Itzler, M. A., Bienfang, J. C., and McIntosh, K. A., eds., **11386**, 113860N, International Society for Optics and Photonics, SPIE (2020).

[13] Kuzmenko, K., Vines, P., Halimi, A., Collins, R. J., Maccarone, A., McCarthy, A., Greener, Z. M., Kirdoda, J., Dumas, D. C. S., Llin, L. F., Mirza, M. M., Millar, R. W., Paul, D. J., and Buller, G. S., "3d lidar imaging using ge-on-si single–photon avalanche diode detectors," *Opt. Express* **28**, 1330–1344 (Jan 2020).

[14] Millar, R. W., Kirdoda, J., Thorburn, F., Yi, X., Greener, Z. M., Huddleston, L., Benakaprasad, B., Watson, S., Coughlan, C., Buller, G. S., and Paul, D. J., "Pseudo-planar Ge-on-Si single-photon avalanche diode detector with record low noise-equivalent power," in [*Quantum Technology: Driving Commercialisation of an Enabling Science II*], Padgett, M. J., Bongs, K., Fedrizzi, A., and Politi, A., eds., **11881**, 118810F, International Society for Optics and Photonics, SPIE (2021).

[15] Song, J., Yuan, S., Cui, C., Wang, Y., Li, Z., Wang, A. X., Zeng, C., and Xia, J., "High-efficiency and high-speed germanium photodetector enabled by multiresonant photonic crystal," *Nanophotonics* **10**, 1081–1087 (Dec. 2020).

[16] Song, J., Bin, S., Zhou, C., and Qin, B., "High-performance normal-incidence ge/si meta-structure avalanche photodetector," *Photonics* **10**, 780 (July 2023).

[17] Yezekyan, T., Zenin, V. A., Thomaschewski, M., Malureanu, R., and Bozhevolnyi, S. I., "Germanium metasurface assisted broadband detectors," *Nanophotonics* **12**, 2171–2177 (May 2023).

[18] Varshni, Y., "Temperature dependence of the energy gap in semiconductors," *Physica* **34**, 149–154 (Jan. 1967).

[19] Lucarini, V., Peiponen, K.-E., Saarinen, J. J., and Vartiainen, E. M., "Kramers-kronig relations and sum rules in linear optics," *Kramers-Kronig relations in optical materials research* , 27–48 (2005).

[20] Powell, M. J. D., [*A Direct Search Optimization Method That Models the Objective and Constraint Functions by Linear Interpolation*], 51–67, Springer Netherlands (1994).

[21] McIntyre, R., "On the avalanche initiation probability of avalanche diodes above the breakdown voltage," *IEEE Transactions on Electron Devices* **20**(7), 637–641 (1973).

[22] Van Overstraeten, R. and De Man, H., "Measurement of the ionization rates in diffused silicon p-n junctions," *Solid-State Electronics* **13**, 583–608 (May 1970).

[23] Hurkx, G., de Graaff, H., Kloosterman, W., and Knuvers, M., "A new analytical diode model including tunneling and avalanche breakdown," *IEEE Transactions on Electron Devices* **39**(9), 2090–2098 (1992).

[24] Hurkx, G. A., Klaassen, D. B., Knuvers, M. P., and O'Hara, F. G., "A new recombination model describing heavy-doping effects and low-temperature behaviour," *Technical Digest - International Electron Devices Meeting* , 307–310 (1989). SRH and BTBT generation.

[25] Smith, C., Kirdoda, J., Dumas, D., Coughlan, C., McCarthy, C., Mowbray, H., Mirza, M., Fleming, F., Yi, X., Saalbach, L., Buller, G., Paul, D., and Millar, R., "Simulation and design optimization of germanium-on-silicon single photon avalanche diodes," in [*Silicon Photonics XVIII*], Reed, G. T. and Knights, A. P., eds., SPIE (Mar. 2023).